Accepted Manuscript

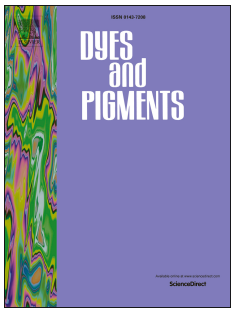

Conjugated dyes carrying N, N*N, N*-dialkylamino and ketone groups: One-component visible light Norrish type II photoinitiators

Ge Ding, Chuan Jing, Xiaozhuan Qin, Yulong Gong, Xueping Zhang, Shengtao Zhang, Ziping Luo, Hongru Li, Fang Gao

PII: S0143-7208(16)31041-5

DOI: 10.1016/j.dyepig.2016.10.034

Reference: DYPI 5550

To appear in: *Dyes and Pigments*

Received Date: 6 June 2016

Accepted Date: 24 October 2016

Please cite this article as: Ding G, Jing C, Qin X, Gong Y, Zhang X, Zhang S, Luo Z, Li H, Gao F, Conjugated dyes carrying N, N*N, N*-dialkylamino and ketone groups: One-component visible light Norrish type II photoinitiators, *Dyes and Pigments* (2016), doi: 10.1016/j.dyepig.2016.10.034.

Conjugated dyes carrying N, N-dialkylamino and ketone groups: one-component visible light Norrish type II photoinitiators

Ge Ding, Chuan Jing, Xiaozhuan Qin, Yulong Gong, Xueping Zhang, Shengtao Zhang[1,2*], Ziping Luo[1,2*], Hongru Li[1,2*], Fang Gao[1,2*]

[1]College of Chemistry and Chemical Engineering, Chongqing University, Chongqing, China, 400044

[2]National-municipal Joint Engineering Labrotory for Chemical Process Intensification and Reaction, Chongqing University, Chongqing, China, 400044

Tel/Fax: 86-23-65102531, Emails: stzhang@cqu.edu.cn, zpluo@126.com, hrli@cqu.edu.cn, fanggao1971@gmail.com

Abstract

This work presents new conjugated dyes carrying N, N-dialkylamino and ketone groups for using as one-component Norrish type II visible light photoinitiators. The novel dyes without ketone group were also synthesized to compose two-component visible light photoinitiators for comparisons. The target dyes show the remarkable absorption in visible light region. Photo-differential scanning calorimetry was employed to study visible light photoinitiating polymerization kinetics of methyl methacrylate by new one-component photoinitiators and two-component photoinitiators respectively. The results suggest that the one-component photoinitiators showed much more efficient photoinitiating polymerization of methyl methacrylate than the two-component photoinitiating systems under visible light irradiation. The molecular weight of visible light photopolymer produced by the new photoinitiators was determined. The visible light photoinitiating mechanism of the one-component photoinitiators was studied by absorption and emission spectra, electron spin resonance spectra and cyclic voltammograms analysis.

Keywords: Norrish type II photoinitiator; Visible light phtotopolymerization; Photopolymerization kinetics; Free radical; Electron transfer; Acrylate monomers

1. Introduction

In recent decades, the study of photoinitiating polymerization of monomers has been receiving considerable attentions since it has wide applications such as microelectronic circuits, printing plates, automobile coating, dental clinical and so on[1-4]. In general, photoinitiating polymerization is finished through three steps: (a) a photoinitiator is excited by light irradiation firstly, (2) and then the active free radicals are yielded, and (3) in the end, monomer is initiated for photopolymerization by consuming free radicals. This process reflects that photoinitiators play central roles in the achievement of efficient photopolymerization.

Normally, photoinitiators can be divided into bond α-cleavage type (Norrish type I) or hydrogen abstraction type (Norrish type II) [5, 6]. Type I is a class of the molecule which yields free radicals by direct cleavage reaction under light irradiation. For example, 2-hydoxy-2-methyl-1-phenyl-propan-1-one is representative type I photoinitaitor [7]. While Norrish Type II is a group of the compound that produces free radicals through direct hydrogen abstraction under irradiation of light. For instance, thioxanthones and benzil are well-known type II photoinitaitors [8]. Considering chemical stability and blocking effect, Norrish type II photoinitiators possess more advantages for photoinitiating polymerization of monomers.

However, the most of both Norrish type I and type II photoinitiators such as Irgacure 819 and benzophenone only absorb 200~300 nm light, and they cannot produce free radials for photoinitiating polymerization of monomers under visible light irradiation (≥ 400 nm light source). Hence, some long wavelength dyes are often employed as photosensitizers to sensitize UV photoinitiators through intermolecular electron transfer to yield active free radials for photopolymerization of monomers under visible light irradiation [9, 10]. A number of efforts have been devoted to develop new long-wavelength photosensitizers for visible light

photopolymerization [11]. For example, some squaraine dyes can efficiently photosensitize iodonium salt to produce free radicals for photopolymerization of monomers under visible light irradiation [12].

This method is conveniently applied since a library of long wavelength organic dyes can act as photosensitizers. However, photoinduced intermolecular electron transfer between a long wavelength photosensitizer and a UV photoinitiator is limited by a number of factors including compatibility, polarity as well as viscosity of the systems. In particular, with the progress of the photopolymerization, photosensitizer molecules and UV photoinitiator molecules could be separated by yielded photopolymeric materials. As a consequence, photoinitiating polymerization efficiency of monomers under long wavelength irradiation by this approach needs to be improved.

Hence, photoinduced internal electron transfer is proposed to achieve more efficient long wavelength photoinitiating polymerization [13, 14]. This requires that a photoinitiator can not only absorb visible light efficiently, but also produce free radicals greatly through a ultrafast photoinduced intramolecular electron transfer under visible light irradiation. However, it is a quite challenge to prepare one-component visible light photoinitiators on the basis of rational molecular design.

It is a useful strategy to get long wavelength photoinitiators based on molecular preorganization of dye-attached UV photoinitiaors via covalent bonds. For instance, some attempts have been made to synthesize chloromethyl-1,3,5-triazine-attached cyanine dyes as visible light photoinitiators [15]. To such a molecule, cyanine dye part absorbs visible light firstly, and then electron is transferred to chloromethyl-1,3,5-triazine segment through the linker, and the free radicals are yielded through bond cleavage reaction for photoinitiating polymerization of

monomers. It is obvious that these molecules are regarded as Norrish type I visible light photoinitators.

While so far, there are few studies on Norrish type II visible light photoinitiators due to the more difficulty in the molecular preconstruction. Arsu etal reported a thioxanthone-based fused multi aromatic ring as a visible photoinitiator [16]. However, it required the other component tertiary alkyl amine as the coinitiator to photoinitiate acrylate monomers together under visible light irradiation. If without the coinitiators, visible light photoinitiating of acrylate monomers is hard to occur. In addition, the rigid fused aromatic ring of the target photoinitiator lowers the solubility and the compatibility with the other components in formulation.

Inspired by these efforts, this study proposes to develop well-conjugated photoinitiators carrying N, N-dialkylamino and ketone groups. The presence of phenyl keto moiety means that the target molecules could be used as Norrish type II photoinitiators. N, N-Dialkylamino groups play the followings roles: (1) a tertiary amine group in target dyes act as a hydrogen donor to produce active free radicals for visible photoinitiating polymerization of monomers [17, 18]; (2) it favors the extension of the absorption wavelength of the target photoinitiators due to electron-donating properties; (3) it increases photoinduced internal electron transfer, which is favorable for the yields of free radicals [19]; and (4) it can improve the compatibility of target visible photoinitators with the other formulation components [20, 21].

Furthermore, the good π conjugated structure of the target molecules could lead to the red-shift of absorption wavelength as well as the improvement of photoinduced intramolecular electron transfer. Hence, the more efficient visible light photoinitiating polymerization of acrylated monomers by the new target dyes can be expected.

In this study, photo-differential scanning calorimetry (photo-DSC) was employed to study visible light photoinitiating polymerization kinetics of monomers by the target photoinitiators. Meanwhile, the corresponding new photosensitizers without ketone group were also prepared as the references to compose two-component visible light photoinitiators for the comparisons. The results show that the new one-component visible light photoinitiators could photoinitiate polymerization of acrylate monomers more efficiently than two-component ones. This study can guide us to develop new visible light Norrish type II one-component photoinitiators for free radical polymerization of acrylate monomers through rational molecular preorganization.

2. Experimental

2.1. Materials and characterization

The organic solvents supplied by Aldrich Corporation were dried according to standard laboratory procedures [22]. The monomer methyl methylacetate (MMA) was redistilled in vacuum prior to use, which was purchased from Aldrich. The new visible photoinitiators including 4-benzoyl-4'-dimethylamino-diphenylethylene (**C1**), 4-benzoyl-4'-diethylamino-diphenylethylene (**C2**), and 4-benzoyl-4'-dibutylamino-diphenylethylene (**C3**) were prepared in our laboratory (**Scheme 1**). The novel visible light photosensitizers consisting of dimethyl-(4-(2-(4-styryl-phenyl)-vinyl)-phenyl)-amine (**C4**), diethyl-(4-(2-(4-styryl-phenyl)-vinyl)-phenyl)-amine (**C5**) and dibutyl-(4-(2-(4-styryl-phenyl)-vinyl)-phenyl)-amine (**C6**) were also synthesized in our laboratory (**Scheme 1**). The starting materials for the synthesis of these new target molecules were obtained

from Acros Corporation. Nuclear magnetic resonance (NMR), elemental analysis as well as X-ray single crystal diffraction were used to characterize chemical structures of the target molecules.

Insert Scheme 1

^{1}H- & ^{13}C- NMR spectra of the samples were determined in deuterated solvents by a Bruker 500 MHz spectrometer at room temperature. Tetramethysilance (TMS) was used as an internal standard to identify NMR chemical shifts of the samples. Elemental analysis of the samples was performed by a CE440 from Exeter Analytical Inc apparatus. The melting points of the samples were studied by a X-5 apparatus from Beijing Focus Instrument Co. Ltd.

Single crystals of the target dyes were obtained by a slow volatilization of organic solvents in NMR tube. X-ray diffraction data were acquired by a Bruker-AXS CCD area detector equipped with diffractometer with Mo K_a (λ = 0.71073 Å) at 298 K. A suitable single crystal was put inside a glass fiber capillary to determine the structure through direct methods which were refined by full-matrix least squares on F^2. All the hydrogen atoms were labeled in calculated positions respectively and all the non-hydrogen atoms were introduced by anisotropic temperature factors.

2.2. Static and transient absorption and emission spectra

A Cintra spectrophotometer was employed to determine the static UV/visible absorption spectra of the samples. The fluorescence emission spectra of the samples (2×10^{-6} mol/L) were determined by F-531PC spectrofluorophotonmeter. Quinine sulfate in 0.5 mol/L H_2SO_4 (Φ, 0.546) was used as the reference to measure the fluorescence quantum yields of the samples [23].

A 355 nm nanosecond laser was used to perform laser flash photolysis measurements, which were conducted in a rectangular quartz cell with a path length of 5 mm along the monitoring light path. In a dark room, the samples were deaerated by bubbling with argon for one hour before laser

detection. The transmitted monitoring light from the samples was collected and focused onto a monochromator, which was processed by a computer system.

2.3. Photopolymerization kinetics study by Photo-DSC

Photo-DSC-204 F1 phoneix from Netzsch Corporation of Germany was used to evaluate the visible light photoinitating polymerization kinetics of MMA photoinitiated by the studied systems. A high pressure mercury lamp was used as the light source. The wavelength above 400 nm light was allowed to go through by cutting UV wavelength light through a filter.

An open aluminum pan with a diameter of 6.6 mm contained the formulation components for visible light photoinitiaited polymerization, and an empty aluminum pan was employed as the blank. The photoinitiating polymerization mixture was cooled in a nitrogen flow of 60 mL/ min under visible light irradiation. The average power of visible light irradiation was 20 mW/cm^2 measured by a Coherent Model Fieldmaster power meter (Germany). Visible light photopolymerization kinetics of monomer MMA was analyzed by the exothermal plots.

By integrating the area under the exothermic peak, the conversion percent of acrylate double bond (C%):

$$C\%=\Delta H_t / \Delta H_0^{theory} \times 100\% \qquad (1)$$

wherein ΔH_t is the reaction heat at time t, and ΔH_0^{theory} shows the theoretical reaction heat for 100% conversion. ΔH_0^{theory} is 86 kJ/mol for an acrylic double bond [24]. The rate of polymerization (R_p) is directly related to the heat flow *dH/dt* by the following equation:

$$R_p=dC/dt=(dh/dt)/\Delta H_0^{theory} \qquad (2)$$

2.4. Cyclic voltammograms determination

Shanghai Chenhua electrochemical work station was used to determine cyclic voltammograms of the samples. A representative three-electrode system including two platinum work electrodes and an Ag/AgCl reference electrode were put in a cell for measurements of cyclic voltammograms. A 0.05 mol/L solution of tetra-n-butyl-ammonium hexafluorophosphate in dichloromethane containing the samples was bubbled with argon for 30 min.

2.5. Gel permeation chromatography (GPC) analysis

Gel permeation chromatography (GPC) was used to determine molecular weights of photopolymer PMMA produced in this work. Variations of molecular weights (number average molecular weight, M_n, weight average molecular weight, M_w) and polydispersity index (PDI) of polymethyl methacrylate (PMMA) were acquired by a Shimadzu GPC instrument with tetrahydrofuran (HPLC grade, Sigma-Aldrich Co, USA) as the mobile phase at a low rate of 1 mL/min.

The photopolymer PMMA was yielded by the studied visible light photoinitiating systems, which was precipitated in cold methanol, and dried in vacuum. The polydispersity of the above PMMA based on molecular weight according to the following equation:

$$M_w/M_n=1+P \qquad (3)$$

wherein P represents the extent of the polymerization reaction.

2.6. Electron spin resonance (ESR) analysis

Bruker EMX EPR spectrometer at 9.5 GHz with a modulation frequency of 200 KHz was employed to perform electron spin resonance (ESR) with 5, 5-dimethyl-pyrroline-N-oxide (DMPO) as the radical capturing agent. A high-pressure mercury lamp was used as the light source in ESR spectrometer cavity. The concentrations of the components in organic solvents

were 5×10^{-4} mol/L, and then 0.5 mL of each sample was placed into a quartz ESR tube and then purged with nitrogen for half an hour to remove oxygen.

2.7. Photobleaching measurements

Photobleaching of the studied visible light photoinitiating polymerization systems was conducted in organic solvents, which were contained in purex tube. The pure argon was bubbled for half an hour to remove oxygen. The 400 W high pressure mercury lamp was used as the light source, and the light below 400 nm wavelength was cut off by a filter to avoid ultraviolet light.

Photobleaching ratios could be calculated by the following equation:

$$w\%=\Delta A/A_0=(A_0 - A_t)/A_0 \qquad (4)$$

wherein A_0 is the optical density at the maximal absorption wavelength before visible light irradiation, and A_t represents the absorption at 400 nm after (t) time irradiation of visible light.

2.8. Preparation of the target molecules

Synthesis of **C1**~**C3**

Intermediate 1, (4-bromomethyl-phenyl)-phenyl-methanone

4-Methylbenzophenone 10.0 g (0.05 mol) and azodiisobutyronitrile (AIBN, 0.075 g) was added to 150 ml CCl_4 in a round bottom flask with a condenser and a magnetic stirrer, and then N-bromosuccinimide (NBS, 9.0 g, 0.05 mol) was added. The mixture was keep refluxing for 24 h, then was cooled to room temperature, the solvent was evaporated under vacuum in the end. The product was further purified through recrystallization from benzene and cyclohexane to yield white solid (yield, ~59%, m.p., 103.0~105.0 °C). ^{1}H-NMR (500 MHz, $CDCl_3$) δ (ppm)：4.456 (s, -CH_2, 2H), 7.18-7.20 (d, Ar-H, 2H), 7.532-7.534 (d, Ar-H, 2H), 7.425-7.434 (d, Ar-H, 2H), 7.505-7.519 (t, Ar-H, 1H), 7.711-7.725 (d, Ar-H, 2H). ^{13}C-NMR (125 MHz, $CDCl_3$) δ (ppm):

38.323, 124.652, 126.863, 129.832, 130.083, 133.843, 135.083, 135.326, 139.093, 187.083. Elementary analysis, Anal. Calcd for $C_{14}H_{11}BrO$: C, 61.12; H, 4.03. Found: C, 61.02; H, 3.97.

Intermediate 2, (4-benzoyl-benzyl)-phosphonic acid diethyl ester

In a three-necked flask equipped with a magnetic stirrer, (4-bromomethyl-phenyl)-phenyl-methanone (1.1 g, 4 mmol) and triethylphosphite (6.6 ml) were added with molar ratio of 1:10. The mixture was heated to 130-160 ℃ for 5 hours under stirring, After the reaction, The triethylphosphite was removed under reduced pressure to provide the crude product (yield , ~95%). ^{1}H-NMR (500 MHz, $CDCl_3$) δ (ppm)：1.046-1.336 (t, -CH_3, 6H), 3.062 (s, -CH_2, 2H), 3.824-3.930 (m, -OCH_2, 4H), 7.210-7.245 (m, Ar-H, 2H), 7.245-7.281 (d, Ar-H, 2H), 7.338-7.385 (d, Ar-H, 3H), 7.530-7.584 (m, Ar-H, 2H). ^{13}C-NMR (125 MHz, $CDCl_3$) δ (ppm): 14.293, 31.038, 61.937, 127.093, 127.973, 130.274, 130.285, 131.093, 133.072, 135.528, 138.049, 187.938. Elementary analysis, Anal. Calcd for $C_{18}H_{21}O_4P$: C, 65.04; H, 6.38. Found: C, 65.12; H, 6.25.

C1, 4-benzoyl-4'-dimethylamino-diphenylethylene

Diethyl-4-benzoylbenzylphosphonate and sodium methoxide (4 mmol, 0.216 g) was added to 40 ml THF in a round bottom flask. 4-(Dimethylamino)-benzaldehyde (3.5 mmol) was added into the mixture, and then kept stirring for 18~24 h at room temperatures. After the reaction was finished, the mixture was cooled to room temperature. After the solvent was evaporated under vacuum, the mixture was further purified by column chromatography (benzene/ethyl acetate, 30/1, v/v) and recrystallization from benzene and cyclohexane to give yellow solid (yield, ~66%, m.p., 186~187 °C). ^{1}H-NMR (500 MHz, $CDCl_3$) δ (ppm): 3.00 (s, -CH_3, 6H), 6.79 (s, Ar-H, 2H), 6.96 (d, J=16 Hz, Ar-CH=CH, 1H), 7.18 (d, J=16 Hz, Ar-CH=CH, 1H), 7.47(m, Ar-H, 4H), 7.56 (m, Ar-H, 3H), 7.80 (m, Ar-H, 4H). ^{13}C-NMR (125 MHz, $CDCl_3$) δ (ppm): 40.413, 112.569, 123.070,

125.288, 127.686, 127.831, 29.483, 130.405, 131.063, 131.714, 134.967, 137.659, 142.073, 150.305, 195.702. Elementary analysis, Anal. Calcd for $C_{23}H_{21}NO$: C, 84.37; H, 6.46; N, 4.28. Found: C, 84.25; H, 6.37; N, 4.17.

C2, 4-benzoyl-4'-diethylamino-diphenylethylene

The synthesis of **C2** followed the same procedure as described that of **C1**, in which 4-(dimethylamino)-benzaldehyde was replaced by 4-(diethylamino)-benzaldehyde in the last step. The product of yellow solid was obtained (yield, ~69%, m.p., 110~111 °C). ^{1}H-NMR (500 MHz, $CDCl_3$) δ (ppm): 1.19 (t, J=7 Hz, -CH_3, 6H), 3.39 (m, Ar-CH_2, 4H), 6.67 (d, J=9 Hz, Ar-H, 2H), 6.92 (d, J=16.5 Hz, Ar-H, 1H), 7.18 (d, J=16.5 Hz, Ar-CH=CH, 1H), 7.42 (m, Ar-CH=CH, 2H), 7.49 (m, Ar-CH=CH, 2H) 7.56 (m, Ar-H, 3H), 7.80 (m, Ar-H, 4H). ^{13}C-NMR ($CDCl_3$, 125 MHz): 12.702, 44.449, 111.633, 122.284, 123.994, 125.575, 128.259, 128.400, 129.912, 130.860, 131.850, 132.094, 135.090, 138.186, 142.878, 147.950, 196.103. Elementary analysis, Anal. Calcd for $C_{25}H_{25}NO$: C, 84.47; H, 7.09; N, 4.50. Found: C, 84.39; H, 7.16; N, 4.61.

C3, 4-benzoyl-4'-dibutylamino-diphenylethylene

The synthesis of **C3** followed the same procedure basically as described that of **C1**, in which 4-(dimethylamino)-benzaldehyde was replaced by 4-(dibutylamino)-benzaldehyde in the last step. The solid pale yellow product was obtained (yield, ~60%, m.p., 108.9~110.6 °C). ^{1}H-NMR (500 MHz, $CDCl_3$) δ (ppm): 1.03 (t, J= 7.25 Hz, -CH_3, 6H), 1.42 (m, -CH_2-, 4H), 1.64 (m, -CH_2-, 4H), 3.35 (t, J=7.75 Hz, Ar-CH_2-, 4H), 6.69 (d, J=8.5 Hz, Ar-H, 2H), 6.97 (d, J=16.0 Hz, Ar-CH=CH, 1H), 7.23 (d, J=16.5Hz, Ar-CH=CH, 1H), 7.47 (d, J=8.5 Hz, Ar-H, 2H), 7.53 (m, Ar-H, 2H), 7.60 (m, Ar-H, 3H), 7.86 (d, J=8.0 Hz, Ar-H, 4H). ^{13}C-NMR ($CDCl_3$, 125 MHz): 14.085, 20.382, 29.515, 50.776, 111.617, 122.160, 123.809, 125.552, 128.237, 128.333, 129.892, 130.838,

131.871, 132.065, 135.023, 138.170, 142.886, 148.350, 195.988. Elementary analysis, Anal. Calcd for $C_{29}H_{33}NO$: C, 84.65; H, 8.02; N, 3.40. Found: C, 84.56; H, 7.93; N, 3.49.

Synthesis of **C4~C6**

Intermediate 3, 1-methyl-4-styryl-benzene

In a three-necked flask equipped with a magnetic stirrer, 4-methyl-benzaldehyde, phenyl acetic acid and piperidine were added with the molar ratio of 1:3:3. The mixture was heated to 100 ℃ for 3 hours with stirring, then the reaction was kept at 130 ℃ for 5 hours. After the reaction, the product was then extracted with CH_2Cl_2 three times. The combined organic layer was dried by anhydrous $MgSO_4$. The solvent was removed under reduced pressure to leave the crude product, which was further purified by column chromatography (*n*-hexane/CH_2Cl_2, 2/1, v/v) to afford the desired product as the yellow needle solid (yield, ~65%, m.p., 146.0~2148.0 ℃). ^{1}H-NMR (500 MHz, $CDCl_3$) δ (ppm): 2.353 (s, -CH_3, 3H), 6.933 (d, J=16.0 Hz, CH=CH, 1H), 7.023 (d, J=16.5 Hz, CH=CH, 1H), 7.153 (d, Ar-H, 2H), 7.231 (t, Ar-H, 1H), 7.278 (d, Ar-H, 2H), 7.294 (d, Ar-H, 2H), 7.324 (m, Ar-H, 2H). ^{13}C-NMR (125 MHz, $CDCl_3$) δ (ppm): 20.438, 121.323, 121.673, 123.634, 124.076, 126.339, 127.032, 127.964, 131.093, 132.532, 135.025. Elementary analysis, Anal. Calcd for $C_{15}H_{14}$: C, 92.74; H, 7.26. Found: C, 92.81; H, 7.13.

Intermediate 4, 1-bromomethyl-4-styryl-benzene

The synthesis of intermediate **4** followed essentially the same procedure as described that of intermediate **1**, where 4-methylbenzophenone was replaced by 1-methyl-4-styryl-benzene in synthetic process. (yield, ~55%, m.p. 106.0～107.8 ℃). ^{1}H-NMR (500 MHz, $CDCl_3$) δ (ppm)：4.476 (s, -CH_2, 2H), 6.934 (d, J=16.5 Hz, CH=CH, 1H), 7.032 (d, J=8.0 Hz, CH=CH, 1H), 7.128 (d, Ar-H, 2H), 7.298 (t, Ar-H, 1H), 7.334 (d, Ar-H, 2H), 7.385 (d, Ar-H, 2H), 7.403 (d, Ar-H, 2H).

^{13}C-NMR (125 MHz, $CDCl_3$) δ (ppm): 37.983, 122.083, 122.487, 124.083, 124.756, 125.932, 128.672, 129.083, 130.483, 130.562, 132.984. Elementary analysis, Anal. Calcd for $C_{15}H_{13}Br$: C, 65.94; H, 4.81. Found: C, 66.02; H, 4.73.

Intermediate 5, (4-styryl-benzyl)-phosphonic acid diethyl ester

The synthesis of crude intermediate **5** followed essentially the same procedure as described that of intermediate **2**, in which (4-bromomethyl-phenyl)-phenyl-methanone was replaced by 1-bromomethyl-4-styryl-benzene in synthetic process. (yield, ~92%). ^{1}H-NMR (500 MHz, $CDCl_3$) δ (ppm): 1.134 (t, J=8.0 Hz, -CH_3, 6H), 3.038 (s, -CH_2, 2H), 3.794 (m, -OCH_2, 4H), 6.932 (d, J=16.0 Hz, CH=CH, 1H), 7.011 (d, J=16.5 Hz, CH=CH, 1H), 7.021 (d, Ar-H, 2H), 7.112 (s, Ar-H, 1H), 7.238 (d, Ar-H, 2H), 7.242 (m, Ar-H, 2H), 7.315 (m, Ar-H, 2H). ^{13}C-NMR (125 MHz, $CDCl_3$) δ (ppm): 14.632, 30.324, 63.283, 123.943, 124.032, 126.847, 127.043, 127.956, 128.043, 128.746, 129.283, 132.094, 133.184. Elementary analysis, Anal. Calcd for $C_{19}H_{23}O_3P$: C, 69.07; H, 7.03. Found: C, 69.15; H, 6.96.

C4, dimethyl-(4-(2-(4-styryl-phenyl)-vinyl)-phenyl)-amine

(4-Styryl-benzyl)-phosphonic acid diethyl ester (3 mmol) and sodium methoxide (3.6 mmol) in 40 ml dry THF were added into 100 ml round bottom flask and stirred at 0℃ for 30 min, 4-(dimethylamino)-benzaldehyde (3.5 mmol, 2.35 g) was added into the mixture as the color was changed to orange. Then, the mixture was stirred for overnight at room temperature. After the reaction was finished, THF was removed under reduced pressure to leave the crude product, which was then purified by column chromatography (benzene/ethyl acetate, 30/1, v/v) and recrystallization from benzene and cyclohexane gave yellow solid (yield, ~65%, m.p., 183.5~184.8 °C). ^{1}H-NMR (500 MHz, $CDCl_3$) δ (ppm): 2.94 (s, -CH_3, 6H), 6.59 (s, Ar-H, 2H),

6.96 (d, J=16.0 Hz, CH=CH, 1H), 7.08 (d, J=8.0 Hz, CH=CH, 1H), 7.11 (d, J=8.0 Hz, CH=CH, 1H), 7.13 (d, J=16 Hz, CH=CH, 1H), 7.24 (m, Ar-H, 2H), 7.28 (m, Ar-H, 2H), 7.33 (m, Ar-H, 1H), 7.40 (m, Ar-H, 2H), 7.63 (m, Ar-H, 4H). ^{13}C-NMR (125 MHz, $CDCl_3$) δ (ppm): 43.423, 114.387, 124.302, 126.273, 126.835, 127.532, 127.873, 128.841, 129.854, 134.632, 134.763, 143.782. Elementary analysis, Anal. Calcd for $C_{24}H_{23}N$: C, 88.57; H, 7.12; N, 4.30. Found: C, 88.61; H, 7.05; N, 4.37.

C5, diethyl-(4-(2-(4-styryl-phenyl)-vinyl)-phenyl)-amine

The synthesis of **C5** followed essentially the same procedure as described that of **C4**, in which 4-(dimethylamino)-benzaldehyde was replaced by 4-(diethylamino)-benzaldehyde in the last step. Recrystallization from CH_2Cl_2 and cyclohexane gave pure material as yellow solid (yield, ~ 43%, m.p. 131.3~133.5°C). ^{1}H-NMR (500 MHz, $CDCl_3$) δ (ppm): 1.13 (t, J=7.0 Hz, -CH_3, 6H), 3.41 (m, -CH_2, 4H), 6.63 (d, J=9.0 Hz, Ar-H, 2H), 6.97 (d, J=16.0 Hz, CH=CH, 1H), 7.11 (d, J=16.5 Hz, CH=CH, 1H), 7.17 (d, J=16.5 Hz, CH=CH, 1H), 7.19 (d, J=16.0 Hz, CH=CH, 1H),7.24 (d, J=16.0 Hz, Ar-H, 2H), 7.212 (t, Ar-H, 1H), 7.33 (m, Ar-H, 2H), 7.42 (m, Ar-H, 2H, 3H), 7.68 (m, Ar-H, 3H). ^{13}C-NMR ($CDCl_3$, 125 MHz) : 13.311, 46.433, 112.754, 123.432, 124.764, 126.126, 126.782, 128.265, 128.922, 133.860, 134.893, 143.932. Elementary analysis, Anal. Calcd for $C_{26}H_{27}N$: C, 88.33; H, 7.64; N, 3.96. Found: C, 88.42; H, 7.57; N, 3.88.

C6, dibutyl-(4-(2-(4-styryl-phenyl)-vinyl)-phenyl)-amine

The synthesis of **C6** followed essentially the same procedure as described that of **C4**, in which 4-(dimethylamino)-benzaldehyde was replaced by 4-(dibutylamino)-benzaldehyde in the last step. Yield, ~63%, m.p., 116.2~117.6 °C. ^{1}H-NMR (500 MHz, $CDCl_3$) δ (ppm): 0.99 (t, J=7.25 Hz, -CH_3, 6H), 1.38 (m, -CH_2-, 4H), 1.53 (m, -CH_2-, 4H), 3.34 (t, J=7.75 Hz, Ar-CH_2-, 4H), 6.59 (d,

J=8.5 Hz, Ar-H, 2H), 6.98 (d, J= 16.5 Hz, CH=CH, 1H), 7.02 (d, J= 16.5 Hz, CH=CH, 1H), 7.13 (d, J= 8.0 Hz, CH=CH, 1H), 7.19 (d, J= 16.0 Hz, CH=CH, 1H), 7.23 (d, J=8.5, Ar-H, 1H), 7.36 (m, Ar-H, 2H), 7.38 (m, Ar-H, 2H), 7.44 (m, Ar-H, 3H), 7.63 (m, Ar-H, 3H). ^{13}C-NMR ($CDCl_3$, 125 MHz): 13.885, 20.125, 31.263, 53.482, 113.617, 124.863, 124.856, 126.522, 126.673, 127.783, 128.073, 128.973, 134.036, 134.733, 144.732. Elementary analysis, Anal. Calcd for $C_{30}H_{35}N$: C, 87.96; H, 8.55; N, 3.42. Found: C, 88.05; H, 8.46; N, 3.49.

3. Results and discussion

3.1 $^{1}H/^{13}C$-NMR spectra of the new target photoinitistors

The synthesis of the target molecules was according to Wittig-Horner reaction through multi-step routes shown in **Scheme 1**. The synthesis strategies provided the advantages such as satisfied yields as well as convenient operations, which produced coplanar trans C-C double bonds.

The representative ^{1}H-NMR and ^{13}C-NMR spectra of **C3** were shown in **Figure 1**. It is found that the chemical shift of $-CH_2$ peaked at b, c and d as well as -CH=CH- peaked at g and h all display remarkably separated peaks because they are not equivalent hydrogen atoms. Triplet peaks at a and d are shown due to the effects of neighboring protons. Furthermore, the chemical shift of H (e) moves to more upfield compared to the other H atoms in phenyl rings since N, N-alkylamino groups possess strong electron donating effects.

Insert Figure 1

In contrast, the electron withdrawing effect of carbonyl group leads to ^{1}H-NMR shift of its adjacent H atoms (j) in phenyl rings to the downfield. Meanwhile, the typical ^{13}C-NMR chemical shift of ketone group is found (**Figure 1**(b), 195.988 ppm). In addition, C-C double bonds show

123.909 and 122.160 ppm (f, g) chemical shifts in ^{13}C-NMR spectra. In summary, the ^{1}H-NMR and ^{13}C-NMR spectra suggest that benzophenone was successfully covalently attacted to the dye by C-C double bonds. The other tagret photoinitistors **C1** and **C2** show the similar ^{1}H-NMR and ^{13}C-NMR spectra (typically shown in，**Figure S1, Supplementary data**).

As a matter of fact, the other multi-step synthesis routes using Wittig-Horner reaction have also been successful established to prepare the target dyes in our lab (**Scheme 2**). Hence, it is feasible to obtain a large scale preparation of the target dyes for the future application.

Insert Scheme 2

The single crystal of **C1** was prepared by a slow evaporation of mixed organic solvents. X-ray single crystal diffraction analysis and molecular π-π stacking structure demonstrate that C-C double bond in **C1** shows neat trans-configuration (**Figure 2**). In addition, the small dihedral angle (∠C28-C31-C32-C33) around C-C double bond (3.02 °) indicates that π conjugation part in **C1** possess the great coplanarity (see **Supplementary data**).

Insert Figure 2

3.2 Static and transient UV/visible absorption and emission

The representative UV/visible absorption spectra of the target molecules **C1**~**C6** in methylene chloride are given in **Figure 3**. It is shown that the maximal absorption wavelengths of these molecules are located in visible light region and the absorption is extended to 500 nm. Furthermore, **C1**~**C3** exhibit a dramatic absorption band around 275 nm, which could be attributed to phenyl keto segment. In contrast, there is absence of remarkable absorption band around 275 nm for **C4**~**C6**.

Insert Figure 3

The typical absorption parameters of these molecules in various solvents are presented in **Table 1**. The data suggest that these molecules yield remarkable absorption in visible light region (ε_{max} at 400 nm, 10^5 magnetitude, $cm^{-1}\cdot mol^{-1}\cdot L$). The absorption maxima of the target molecules show the red-shift with the increase of carbon chain length of N, N-dialkylamino group, which could be ascribed to the enhancement of electron-donating ability with the extended carbon chain.

Insert Table 1

As compared with **C4~C6, C1~C3** show the smaller fluorescence quantum yields (such as in CH_2Cl_2, **C3,** Φ, 0.302, **C6,** Φ, 0.735). This indicates that phenyl keto part could increase the yields of the triplet states of **C1~C3**, in which the initiating radicals are produced. Laser flash photolysis experiments were further conducted to survey the triplet states of photoinitiators. The typical transient absorption spectra of **C3** after the irradiation of laser pulses are provided in **Figure 4**.

Insert Figure 4

It is found that the transients could be efficiently quenched by oxygen, demonstrating that they are ascribed to triplet-triplet absorption. The transient peak around 530 nm is observed under the laser irradiation, which is similar with typical characterization of triplet-triplet spectra of benzophenone [25]. The results further demonstrate that triplet state yields of **C1~C3** are increased by phenyl keto group.

3.3. Visible light photoinitiating polymerization studied by photo-DSC

In this study, two sorts of visible light photoinitiating polymerization systems were studied. The first kind of system included only the new photoinitiator (**C1** or **C2** or **C3**), namely it is a one-component photoinitiating system. While the second type of system was consisted of the new photosensitizer (**C4** or **C5** or **C6**) and the UV photoinitiator benzophenone, meaning it is a

two-component photoinitiating system. The new visible light photoinitiators and photosensitizers exhibited the good compatibility with the other formulations such as monomers in the systems due to the presence of N, N-dialkylamino groups.

The relationships between the conversion percents of double bond of MMA and visible light irradiation time at different concentrations of the photoinitiators **C1**, **C2** and **C3** was investigated by photo-DSC respectively, which was further used to determine the dependence of the photopolymerization rates of MMA on visible light irradiation time.

Figure 5 shows that the conversion percents of double bond of MMA gradually increase with the increase of visible light irradiation time at a fixed concentration of the photoinitiator (such as at 0.05 mol% of **C3**, C%, 6.82%, for 2 s irradiation, C%, 32.3%, for 5 s irradiation). While, the conversion percents of double bond of MMA tend be stable with the further increase of irradiation time (for example at 0.05 mol% of **C3**, C%, 50.3%, for 10 s irradiation, C%, 55.7%, for 15 s irradiation). Meanwhile, the photopolymerization rates of MMA show the increase with the increase of visible light irradiation time (for instance at 0.05 mol% of **C3**, Rp (s^{-1}), 0.0312, for 2 s irradiation, Rp (s^{-1}), 0.117 for 5 s irradiation), but they decrease from the peak values with further extension of irradiation time (for example at 0.05 mol% of **C3**, Rp (s^{-1}) , 0.0345, for 10 s irradiation, Rp (s^{-1}) , 0 for 15 s irradiation). This is mostly due to the large consumption of the photoinitiating formulations with further irradiation time [26].

As shown in **Figure 5**, the photoinitiating polymerization rates of MMA increase greatly with the increase of the concentrations of the photoinitiators at the same visible light irradiation time firstly (for example **C3**, at 0.05 mol%, Rp (s^{-1}), 0.116, 0.10 mol%, Rp (s^{-1}), 0.196, for 5 s irradiation). However, the photoinitiating polymerization rates of MMA show small increase as

the concentrations of the photoinitiators are further enhanced (such as **C3**, at 0.15 mol%, Rp (s^{-1}), 0.233, 0.20 mol%, Rp (s^{-1}), 0.278, for 5 s irradiation). As a consequence, the percents of double bond conversion of MMA increase with the increase of the concentrations of photoinitiators firstly (such as **C3,** at 0.05 mol%, C%, 31.9%, 0.10 mol%, C%, 42.8% for 5 s irradiation), and then they show the light increase with further enhancement of the concentrations of the photoinitiators at fixed visible light irradiation time (for example **C3,** at 0.15 mol%, C%, 45.8%, at 0.20 mol%, C%, 48.9% for 5 s irradiation). This could be caused by radical annihilations at the higher concentrations of the photoinitiators [27].

Insert Figure 5

Figure 5 also suggests that the maximal conversion percents of double bond of MMA and the peak photopolymerization rates of MMA increase with the extension of carbon chain length of N, N-dialkylamino groups at the same conditions (such as at 0.20 mol%, **C1**, Rp_{max} (s^{-1}), 0.181, C%, 82.2%, **C2**, Rp_{max} (s^{-1}), 0.213, C%, 84.3%, **C3,** Rp_{max} (s^{-1}), 0.283, C%, 85.4%). The longer alkyl group means the more intensive electron donating effect, yielding the stronger photoinduced intramolecular charge transfer in the photoinitiators. Hence, the free radicals could be produced by **C3** more efficiently under visible light irradiation. It suggests that the electron-donating groups can effectively improve the visible light photoinitiating performance of the photoinitiators.

Insert Figure 6

We also studied visible light photoinitiaing efficiencies of the two-component systems composed by the photosensitizer (**C4**, or **C5** or **C6)** and benzophenone. **Figure 6** shows that the peak conversion percents of double bond of MMA and the maximal photopolymerization rates of MMA produced by the one-component photoinitiators are remarkably greater than those yielded

by the corresponding two-component systems (such as at 0.25 mol% of **C3**, C%, 91.9%, Rp_{max} (s^{-1}), 0.356; at 0.25 mol% of **C6** and 0.25 mol% benzophenone**,** C%, 57.3%, Rp_{max} (s^{-1}), 0.119). The results demonstrate that the free radicals could be produced by the photoinduced internal electron transfer systems more efficiently.

3.4. Molecular weight and polydispersity of photopolymer MMA

The lower value of polydispersity *P* of the produced polymer means the greater extent of the polymerization reaction. For instance, PMMA yielded by **C3** showed the small *P* value (0.569) as its concentration was 1×10^{-5} mol/L under visible light irradiation (M_w, 7.631×10^5, M_n, 4.865×10^5), which is lower than that produced by the corresponding two-component photoinitiating system (**C6** plus benzophenone, *P*, 0.797) at the same experimental conditions. Furthermore, the other one-component photoinitaitors **C1** and **C2** showed the similar results as **C3**. The study suggests that the new one-component photoinitiators (**C1**, **C2** and **C3**) could efficiently photoinitiate polymerization of MMA with a large molecular weight as well as a good polydispersity under visible light irradiation.

3.5. ESR spectra analysis

ESR spectra of the new photoinitiators were determined to analyze visible photoinitiation mechanisms. The active free radicals with the short lifetime formed upon the irradiation could be trapped by DMPO in spin-trapping experiments. **Scheme 3** shows the trapping mechanism of the radicals yielded by the new one-component photoinitiators.

Insert Scheme 3

Typical ESR spectra of **C3** and its corresponding two-component photoinitiating system (**C6** plus benzophenone) are given in **Figure 7**. It shows that the active free radical signals produced

by **C3** system are similar to those yielded by **C6** system. According to **Scheme 3**, α-amine radicals could be recognized by DMPO [28]. It is further found that **C3** shows the greater ESR signal intensities than the two-component **C6** system. As a consequence, the acrylate monomer MMA could be photoinitiated by these one-component photoinitiators more efficiently.

Insert Figure 7

It is considered that N, N-dialkylamino-stilbene part in **C3** undergoes photoinduced intramolecular electron transfer to phenyl keto part under visible light irradiation. Then, an exciplex between the negatively charged transferred species and its ground state could be yielded. In the end, the active α-aminoalkyl free radicals are produced through an intermediate by abstracting hydrogen reaction (**Scheme 4**) [16].

Insert Scheme 4

3.6. Photobleaching studies

The UV/visible absorption of one-component or two-component visible light photoinitiating polymerization systems showed the decreases in organic solvents or solid phase state, which demonstrates photoinduced internal or inter molecular electron transfer leads to the decomposition of the photoinitiators. The representative absorption spectral variations of **C3** system with the visible light irradiation time in CH_2Cl_2 are presented in **Figure 8**, suggesting the occurrence of photobleaching.

Insert Figure 8

The plots of the photobleaching ratios of one-component or two-component photoinitiating systems with the irradiation time are shown in **Figure 9**. The results suggests that **C1** and **C3** systems produce the greater photobleaching rates than **C4** and **C6** systems respectively**,** which

further interprets that **C1** and **C3** undergo the more efficient visible light photoinitiating than **C4** and **C6**. **Figure 9** also shows that **C3** system exhibits the more rapid photobleaching than **C1** one, which further suggests that the stronger electron-donating of N, N-dibutylamino group favors the occurrence of photoinduced electron transfer, and the more efficient visible light photoinitiating polymerization of MMA by **C3** is obtained accordingly.

Insert Figure 9

3.7. The cyclic voltammograms analysis

The cyclic voltammograms of **C1**~**C3** were performed at various scan rates in CH_2Cl_2. The representative cyclic voltammograms of **C3** at the sweeping rates 0.08, 0.1, 0.12, 0.15 and 0.20 V/s is shown in **Figure 10**. It is shown that with the increase of the scan rates, the anodic to cathodic peak current is different from the unity and i_{pa} is not equaled to i_{pc}, which suggests that the redox processes of **C3** are irreversible under all the sweeping rates. In addition, the linear increasing of the peak potentials with the square roots of the scan rates shows that the redox process of **C3** is dominated by the diffusion-controlled electron transfer reactions [29].

Insert Figure 10

The intramolecular electron transfer number of **C3** based on cyclic voltammograms is further calculated. According to Laviron equation [30], the intramolecular electron transfer numbers could be calculated:

$$E_p = E^0 + (1 - \ln \nu) RT / \alpha nF \qquad (5)$$

wherein α shows the cathodic electron transfer coefficient (irreversible process α=0.5), n represents the electron transfer number. R shows the gas constant (R, 8.314 $J \cdot mol^{-1} \cdot K^{-1}$), T is the temperature in Kelvin (T=298K) and F stands for the Faraday constant (F, 96493 $C \cdot mol^{-1}$).

Insert Figure 11

Figure 11 shows the relationship between the peak potentials (E_{pa} and E_{pc}) and the nature logarithm of the sweeping rate (ln*v*). It is shown that the peak potentials are proportionally changed to lnv with a linear regression equation. Hence, n_{pa}=0.736 and n_{pc}=0.730 are obtained, which indicates **C3** could undergo intramolecular negative charge transfer. The study also suggests that an internal charge transfer occurs in **C1** and **C2** as well respectively (**C1**, n_{pa}, 0.696, n_{pc}, 0.692 **C2**, n_{pa}, 0.714, n_{pc}, 0.711). The greater intramolecular electron transfer numbers in **C3** means the more possibility to produce free radicals under visible light irradiation.

4. Conclusions

To be closing, a variety of new conjugated dyes bearing N, N-dialkylamino and ketone groups as Type II one-component visible light photoinitiators are synthesized. The excellent conplanarity of trans C-C double bonds in new target dyes is demonstrated by NMR spectra and X-ray single crystal diffraction. Visible light photoinitiating polymerization of MMA by new one-component photoinitiators are studied by photo-DSC. The results demonstrate that the one-component photoinitiators show much more efficient visible light photoinitiating polymerization of MMA than the corresponding two-component photoinitiating systems. The carbon chain increase of N, N-dialkylamino groups favors the improvement of visible light photoinitiating polymerization of MMA. The presence of phenyl keto segment in molecular skeleton increases the triplet-triplet absorption of the new photoinitiators. The yielded active free radicals by the excited photoinitiators are verified by ESR spectra. The cyclic voltammograms demonstrate that the new photoinitators could undergo intramolecular electron transfer. The

results would guide us to develop new one-component visible light type II photoinitiators as required.

Acknowledgments

The authors greatly thank Natural Science Foundation of Chongqing Projects numbered by CSTC2012jjB50007 and CSTC2010BB0216. H. Li is grateful to the China Postdoctoral Science Foundation for financial supporting (Grant No. 22012T50762 & 2011M501388). We deeply appreciate the support on optical measurements from Key Laboratory of Photochemical Conversion and Optoelectronic Materials, TIPC, Chinese Academy of Sciences.

Supplementary data

X-ray diffraction single crystal data of **C1** (**Table S1~S4**) and **Figure S1** associated with this work are shown in the **Supplementary data**, which are available free of charge from website of this journal. Cif check report of **C1** is also attached to the **Supplementary data**.

The supplementary crystallographic data for this work were also contained in CCDC number 713269, which can be obtained free of charge via http://www.ccdc.cam.ac.uk/conts/retrieving.html or from Cambridge crystallographic data center, 12, Union Road, Cambridge CB2 1EZ, UK; fax: 44-1223-336033.

References

[1] Baikerikar KK, Alec BS. Photopolymerizable liquid encapsulants for microelectronic devices. Polymer 2001; 42: 431-41.

[2] Brömme T, Schmitz C, Oprych D, Wenda A, Strehmel V, Grabolle M, Resch-Genger U, Ernst S, Reiner K, Keil D, Lüs P. Digital Imaging of Lithographic Materials by Radical Photopolymerization and Photonic Baking with NIR Diode Lasers. Chem. Eng. Technol 2006; 39:13-25.

[3] Courtecuisse F, Karasu F, Allonas X, Croutxé-Barghorn C, Van der Ven L. Confocal Raman microscopy study of several factors known to influence the oxygen inhibition of acrylate photopolymerization under LED. Prog. Org. Coat 2016; 92: 1-7.

[4] Song LY, Qiang Y, Ge XP, Anil M, Paulette S. Tris (trimethylsilyl) silane as a co-initiator for dental adhesive:Photo-polymerization kinetics and dynamic mechanical property. Dent. Mater 2016; 32: 102-13.

[5] Shirai M, Okamura H. UV-Curable Positive Photoresists for Screen Printing Plate. Polym. Int 2016; 65: 362-70.

[6] Lauer A, Fast DE, Anne-Marie Kelterer, Elena Frick, Dmytro Neshchadin, Dominik Voll, Georg Gescheidt, and Christopher Barner-Kowollik. Systematic Assessment of the Photochemical Stability of Photoinitiator-Derived Macromolecular Chain Termini. Macromolecules 2015; 48: 8451-60.

[7] Mardyukov A, Studer A. Preparation of Photoactive Polymers and Postmodification via Nitroxide Trapping Under UV Irradiation. Macromol. Rapid. Commun 2013; 34: 94-101.

[8] Kumbaraci V, Aydogan B, Talinli N, Yagci Y. Naphthodioxinone-1, 3-benzodioxole as photochemically masked one-component type II photoinitiator for free radical polymerization. J. Polym. Sci. Part A: Polym. Chem 2012; *50*: 2612-8.

[9] Xiao P, Dumur F, Bui TT, Goubard F, Graff, B, Morlet-Savary F, Fouassier JP, Gigmes, D, Lalevée J. Panchromatic photopolymerizable cationic films using indoline and squaraine dye based photoinitiating systems. ACS Macro Lett. 2013; 8: 736-40.

[10] Nan XY, Huang Y, Fan QG, Shao JZ. Efficient visible photoinitiator containing linked dye-coinitiator and iodonium salt for free radical polymerization. Prog. Org. Coat 2015; 81: 11-8.

[11] Lalevée J, Fouassier JP. Dyes and Chomophores in Polymer Science. John Wiley & Sons, 2015.

[12] He Y, Zhou W, Wu F, Li M, Wang E. Photoreaction and photopolymerization studies on squaraine

dyes/iodonium salts combination. J Photoch Photobio A: Chem 2004; 162: 463-71.

[13] Kawamura K, Yoshimasa A, Hideo T. Photoinduced intramolecular electron transfer between carbazole and bis (trichloromethyl)-s-triazine generating radicals. J Phys Chem B 2003; 107: 4579-86.

[14] Kawamura K. Novel and efficient dye-linked radical generators for visible light photoinitiating polymerization. J Photochem Photobio A Chem 2004; 162: 329-38.

[15] Kawamura K, Kato K. Synthesis and evaluation as a visible‐light polymerization photoinitiator of a new dye-linked bis (trichloromethyl)-1, 3, 5-triazine. Polym Advan Technol 2004; 15: 324-8.

[16] Balta DK, Temel G, Goksu G, Ocal N, Arsu N. Thioxanthone-Diphenyl Anthracene: Visible Light Photoinitiator. Macromolecules 2012; 45: 119-25.

[17] Liu JJ, Chen C, Li ZJ, Wu, WZ, Zhi X, Zhang QG, Hao Wu H, Wang X, Cui SD, Guo K. A squaramide and tertiary amine: an excellent hydrogen-bonding pair organocatalyst for living polymerization. Polym. Chem. 2015; 6: 3754-7.

[18] Aydin M, Arsu N, Yagci Y, Jockusch S, Turro NJ. Mechanistic study of photoinitiated free radical polymerization using thioxanthone thioacetic acid as one-component type II photoinitiator. Macromolecules 2005; 38: 4133-8.

[19] Tasdelen M, Atilla A, Demirel L, Yagci Y. Poly (propylene imine) dendrimers as hydrogen donor in Type II photoinitiated free radical polymerization. Eur. Polym. J 2007; 43: 4423-30.

[20] Yuan J, Lin S, Shen J. Enhanced blood compatibility of polyurethane functionalized with sulfobetaine. Colloids Surf. B: Biointerfaces 2008; 66: 90-5.

[21] Wei J, Liu F, Lu ZM, Song L, Cai DD. Novel PU-type polymeric photoinitiator comprising side-chain benzophenone and coinitiator amine for photopolymerization of PU acrylate. Polym. Adv. Technol 2008; 19: 1763-70.

[22] Perrin D, Armarego W. Purification of Laboratory Chemicals. New York: Pergamon; 1996.

[23] Eaton, DF. Reference materials for fluorescence measurement. Pure & Appl. Chem. 1988; 60: 1107-14.

[24] Jiang X, Luo X, Yin J. Polymeric photoinitiators containing in-chain benzophenone and coinitiators amine: Effect of the structure of coinitiator amine on photopolymerization. J Photochem Photobio A: Chem 2005; 174: 165-70.

[25] Wilkinson F, Willsher CJ. Detection of triplet—triplet absorption in microcrystalline benzophenone by diffuse-reflectance laser flash photolysis. Chem. Phys. Lett 1984; 104: 272-6.

[26] Terrones G, Pearlstein AJ. Effects of optical attenuation and consumption of a photobleaching initiator on local initiation rates in photopolymerizations. Macromolecules 2001; 34: 3195-204.

[27] Musanje L, Ferracane JL, Sakaguchi RL. Determination of the optimal photoinitiator concentration in dental composites based on essential material properties. Dent. Mater 2009; 25: 994-1000.

[28] Wang Y. Jiang X, Yin J. Novel polymeric photoinitiators comprising of side-chain benzophenone and coinitiator amine: Photochemical and photopolymerization behaviors. Eur. Polym. J 2009; 45: 437-47.

[29] Raj C, Retna TO, Ohsaka T. Gold nanoparticle arrays for the voltammetric sensing of dopamine. J. Electroanal. Chem 2003; 543: 127-33.

[30] Luo H, Shi Z, Li N, Gu Z, Zhuang Q.Investigation of the electrochemical and electrocatalytic behavior of single-wall carbon nanotube film on a glassy carbon electrode. Anal Chem 2001; 73: 915-20.

Captions of Schemes, Tables and Figures

Captions of Schemes 1-4

Scheme 1 Synthesis and chemical structures of the target dyes studied in this work

Scheme 2 The other multi-step synthesis routes of the target dyes studied in this work

Scheme 3 The trapping mechanisms of free radicals by DMPO

Scheme 4 The visible light photoinitiated polymerization processing of photoinitiator **C3**

Caption of Table

Table 1 The maximal absorption wavelength of the target molecules in various solvents, the maximal molar extinction coefficient ($10^5 \cdot cm^{-1} \cdot mol^{-1} \cdot L$), Φ, the fluorescence quantum yield

Captions of Figures 1-11

Figure 1 The representative ^1H and ^{13}C NMR spectra of **C3** determined by 500 MHz NMR apparatus in $CDCl_3$

Figure 2 (a) X-ray single crystal diffraction of **C1** ORTEP drawing with 30% possibility of thermal ellipsoids, (b) Single crystal π-π stacking structure of **C1**

Figure 3 Typical UV/visible spectra of **C1~C6** studied in ethyl acetate, the concentration is 1×10^{-5} mol/L respectively

Figure 4 Transient absorption spectra of **C3** in CH_2Cl_2, the concentration is 5×10^{-5} mol/L

Figure 5 (Left/**a1**, **a2**, **a3**) The kinetic curves of visible light photopolymerization of MMA photoinitiated by **C1, C2, C3** respectively at room temperature. and (right/**b1**, **b2**, **b3**) the relationship between the photopolymerization conversion percents of double bond of (-CH=CH-) of MMA and the irradiation time. Irradiation intensity, I_a, 20mW/cm^2.

Figure 6 (Left/**a1, a2, a3**) The kinetic curves of visible light photopolymerization of MMA

photoinitiated by one-component and two-component photoinitiating systems respectively. And (right/**b1**, **b2**, **b3**) the relationship between the photopolymerization conversion percent of double bond (-CH=CH-) of MMA and visible light irradiation time. The concentrations of the photoinitiators, the photosensitizers were 0.25 mol% respectively. Irradiation intensity, 20mW/cm^2

Figure 7 Typical ESR spectra of **C3 (a)** and **C6 (b)** in ethyl acetate.

Figure 8 The variations of UV/visible absorption spectra of **C3** photoinitiating polymerization system with visible light irradiation time, wherein the concentration of **C3** is 1×10^{-5} mol/L, the concentration of MMA is 1×10^{-2} mol/L.

Figure 9 The plots of the photobleaching ratios of various photoinitiating polymerization systems versus the irradiation time

Figure 10 Cyclic voltammetry curves in CH_2Cl_2 of **C3**

Figure 11 The linear relationship between E_{pa}/E_{pc} and lnv of **C3** in methylene chloride

Schemes 1~4

Scheme 1

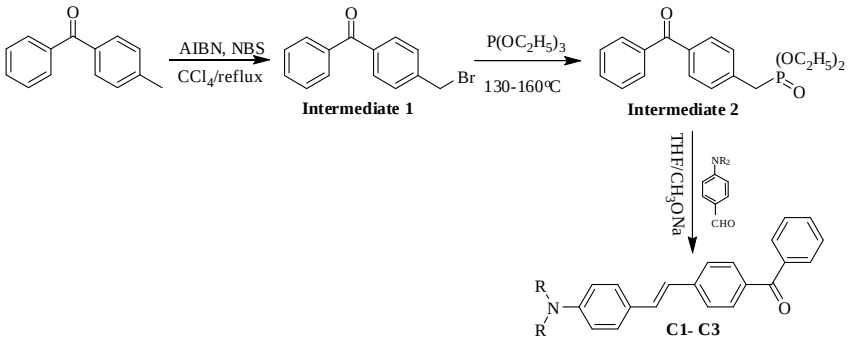

(a)

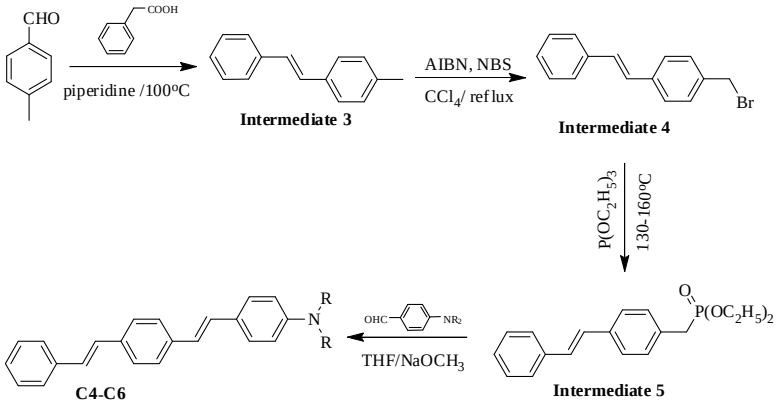

C1, **C4**, R, methyl; **C2**, **C5**, R, ethyl; **C3**, **C6**, R, butyl

(b)

Scheme 2

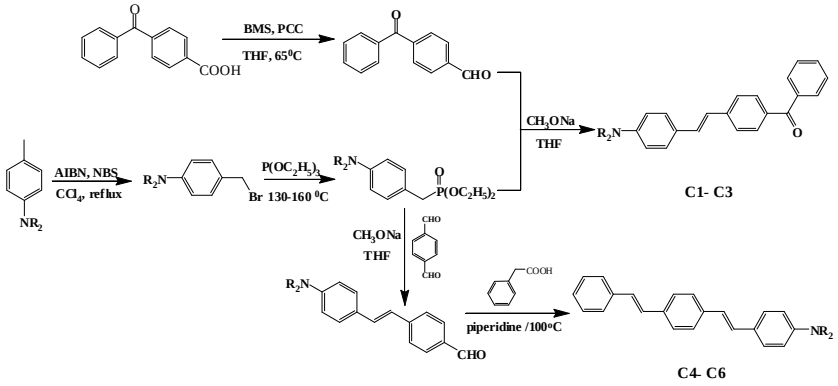

C1, **C4**, R, methyl; **C2**, **C5**, R, ethyl; **C3**, **C6**, R, butyl

Scheme 3

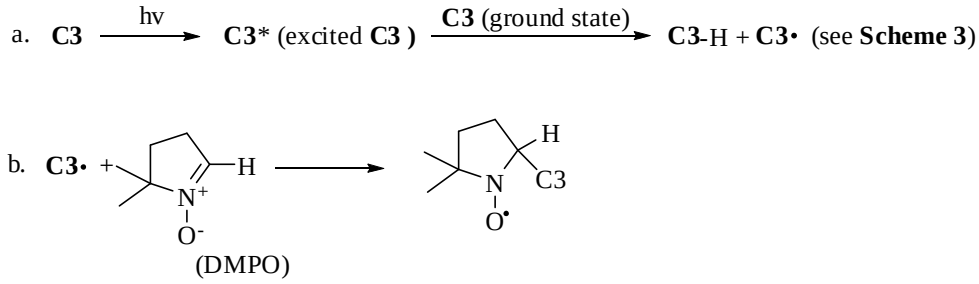

Scheme 4

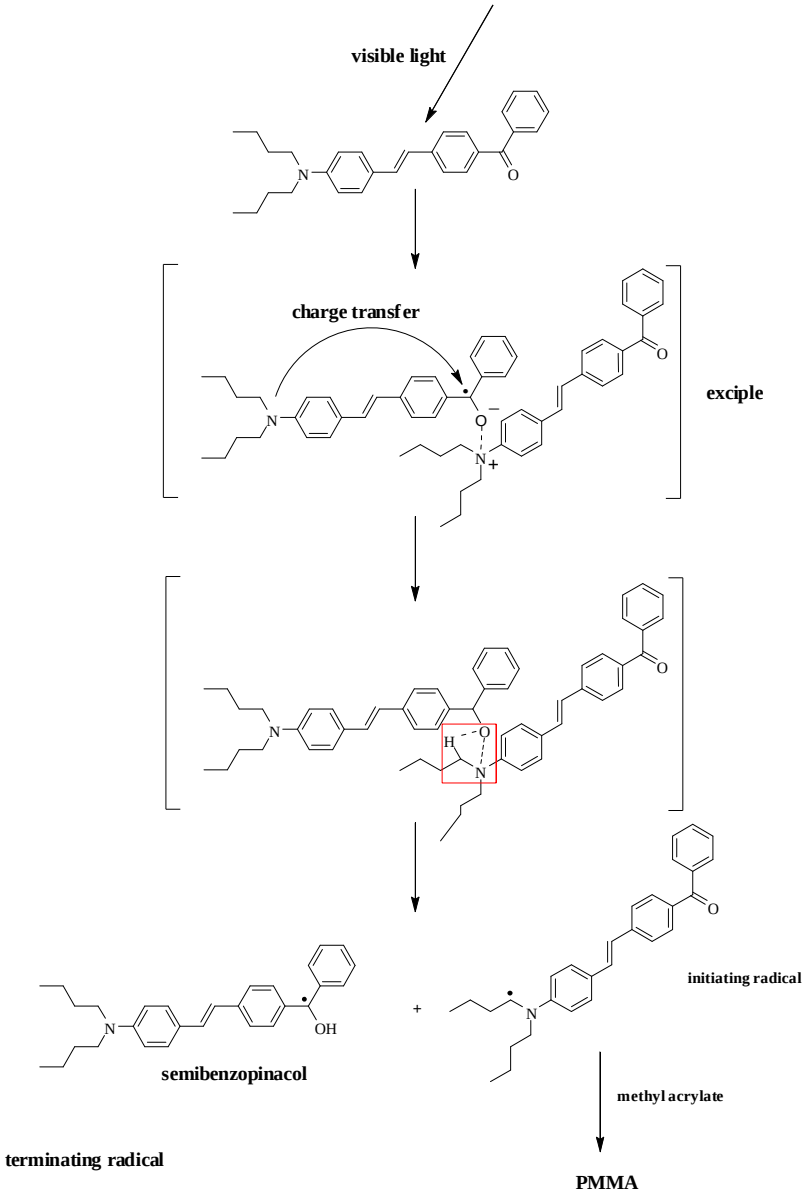

Table 1

Dyes	Solvents														
	Benzene			CH_2Cl_2			THF			EtOAc			ACN		
	λ_{max}	ε_{max}	Φ	λ_{max}	ε_{max}	Φ	λ_{max}	ε_{max}	Φ	λ_{max}	ε_{max}	Φ	λ_{max}	ε_{max}	Φ
C1	398	0.126	0.341	401	0.254	0.231	396	0.272	0.356	392	0.223	0.371	397	0.320	0.302
C2	408	0.187	0.305	415	0.344	0.291	409	0.280	0.363	401	0.248	0.308	410	0.301	0.315
C3	410	0.179	0.353	419	0.258	0.302	411	0.240	0.382	404	0.171	0.294	413	0.411	0.355
C4	403	0.513	0.724	405	0.562	0.799	401	0.528	0.811	400	0.504	0.822	402	0.511	0.798
C5	411	0.508	0.763	417	0.558	0.721	413	0.519	0.835	412	0.492	0.838	418	0.498	0.779
C6	416	0.524	0.772	421	0.573	0.735	423	0.534	0.862	419	0.522	0.849	420	0.535	0.919

Figures 1-11

Figure 1

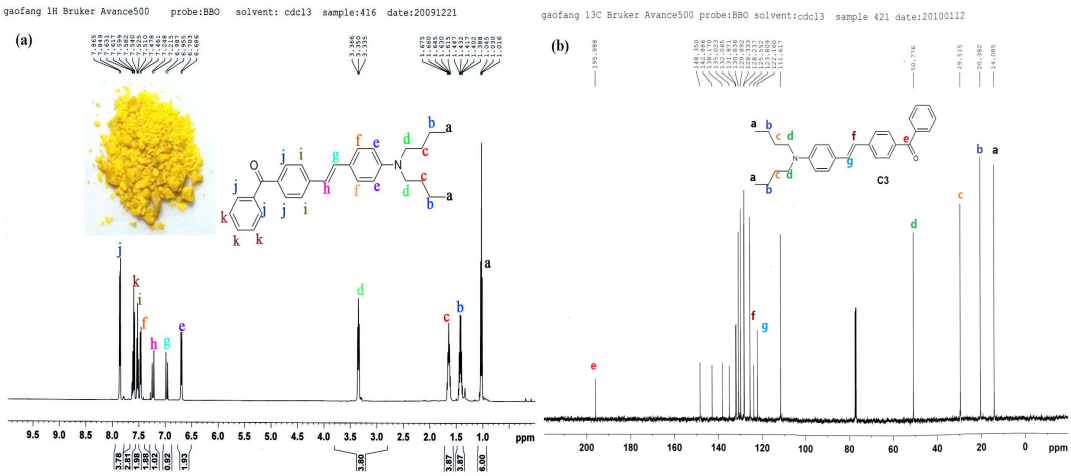

Figure 2

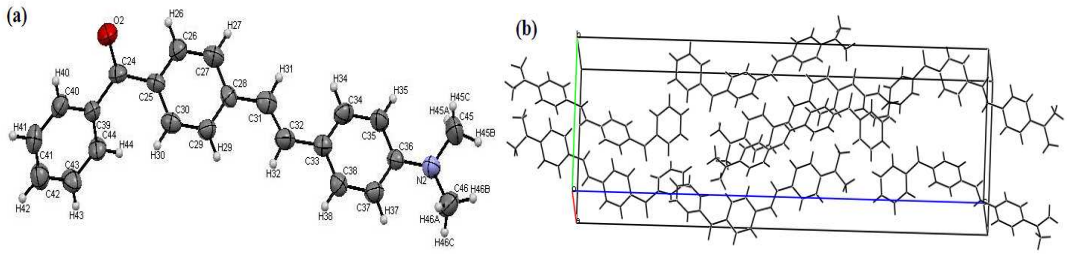

Figure 3

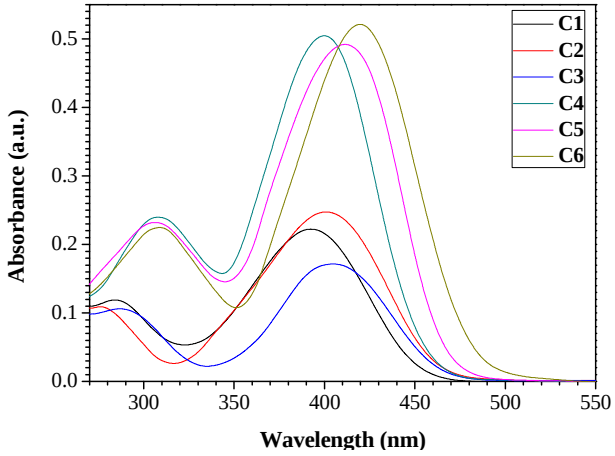

Figure 4

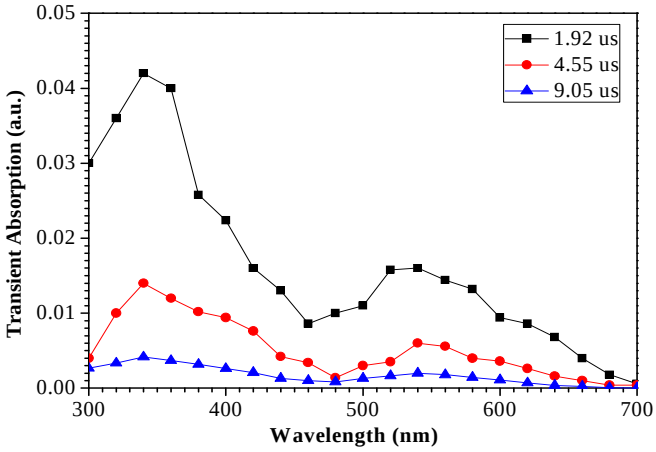

Figure 5

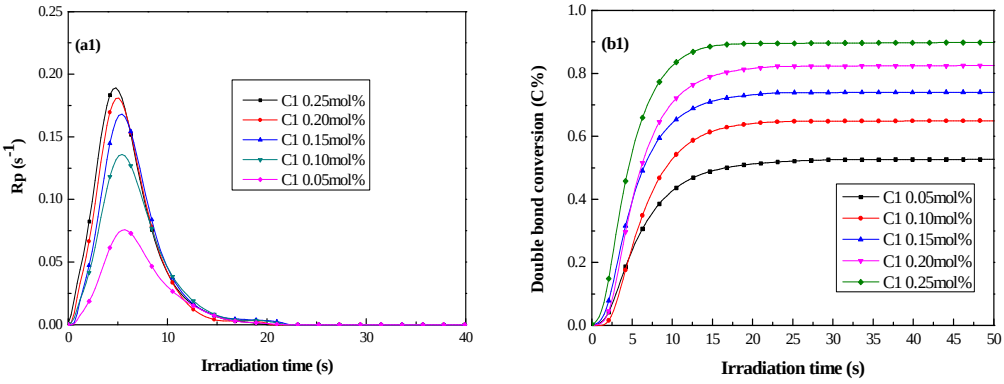

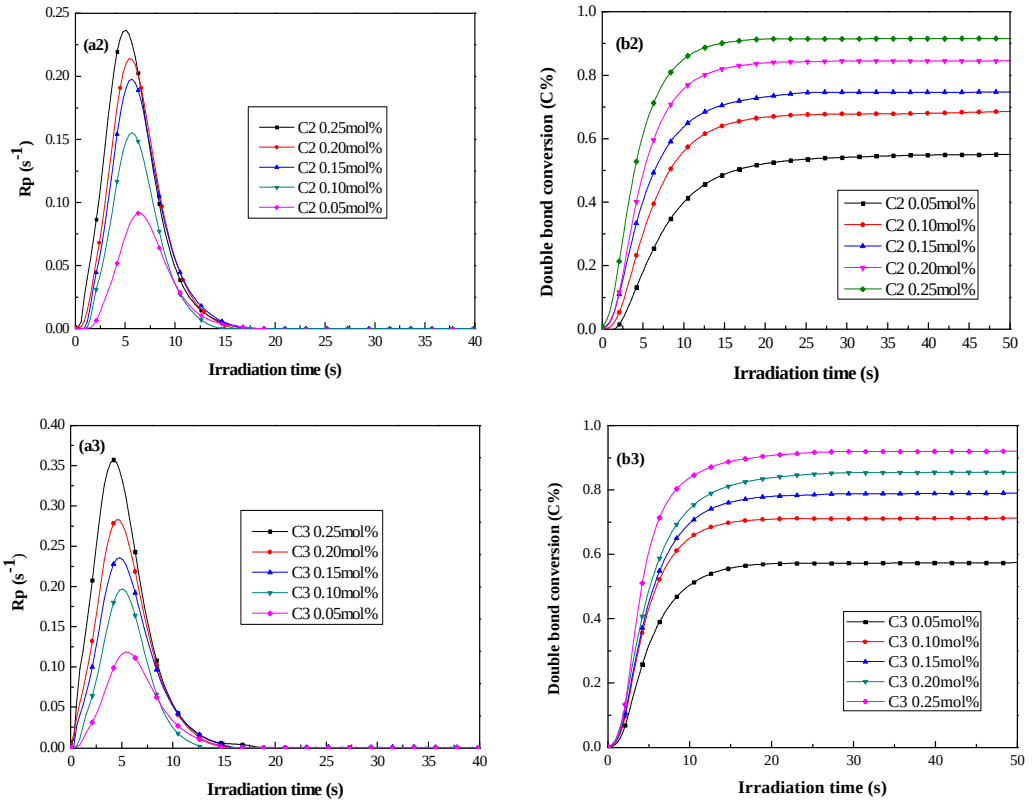
(a2)
Rp (s-1)
Irradiation time (s)
C2 0.25mol%
C2 0.20mol%
C2 0.15mol%
C2 0.10mol%
C2 0.05mol%
(b2)
Double bond conversion (C%)
Irradiation time (s)
C2 0.05mol%
C2 0.10mol%
C2 0.15mol%
C2 0.20mol%
C2 0.25mol%
(a3)
Rp (s-1)
Irradiation time (s)
C3 0.25mol%
C3 0.20mol%
C3 0.15mol%
C3 0.10mol%
C3 0.05mol%
(b3)
Double bond conversion (C%)
Irradiation time (s)
C3 0.05mol%
C3 0.10mol%
C3 0.15mol%
C3 0.20mol%
C3 0.25mol%

Figure 6

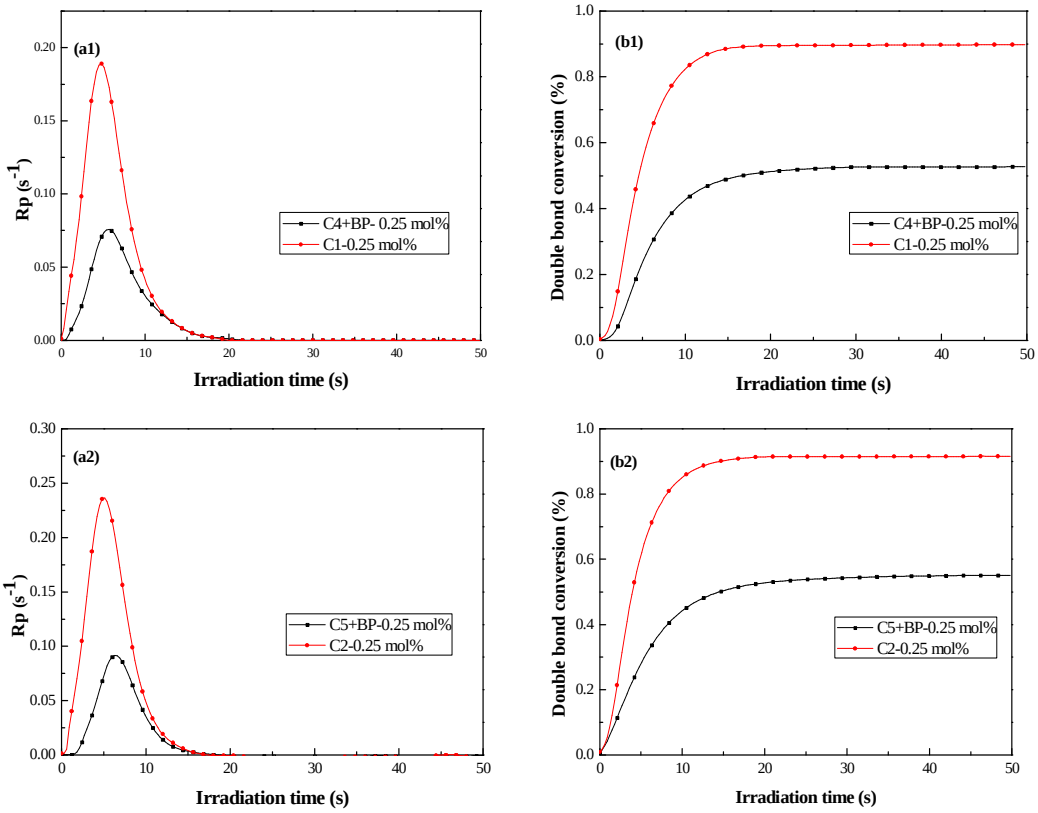
(a1)
Rp (s-1)
Irradiation time (s)
C4+BP- 0.25 mol%
C1-0.25 mol%
(b1)
Double bond conversion (%)
Irradiation time (s)
C4+BP-0.25 mol%
C1-0.25 mol%
(a2)
Rp (s-1)
Irradiation time (s)
C5+BP-0.25 mol%
C2-0.25 mol%
(b2)
Double bond conversion (%)
Irradiation time (s)
C5+BP-0.25 mol%
C2-0.25 mol%

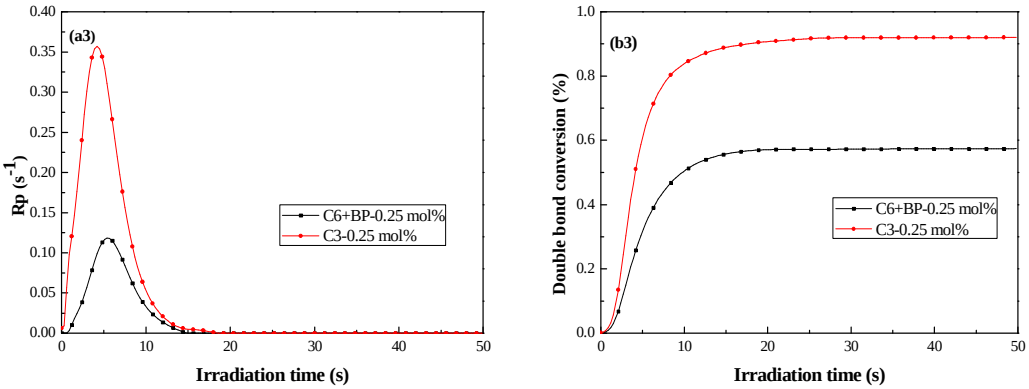

Figure 7

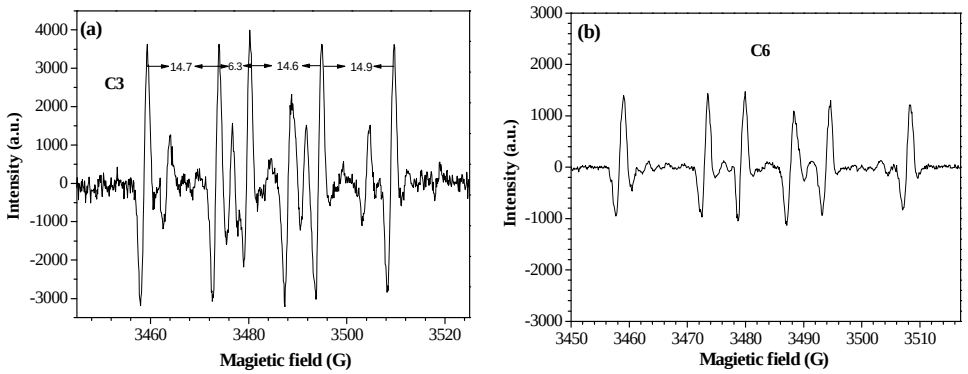

Figure 8

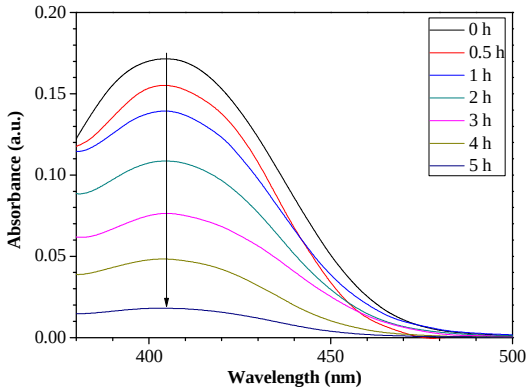

Figure 9

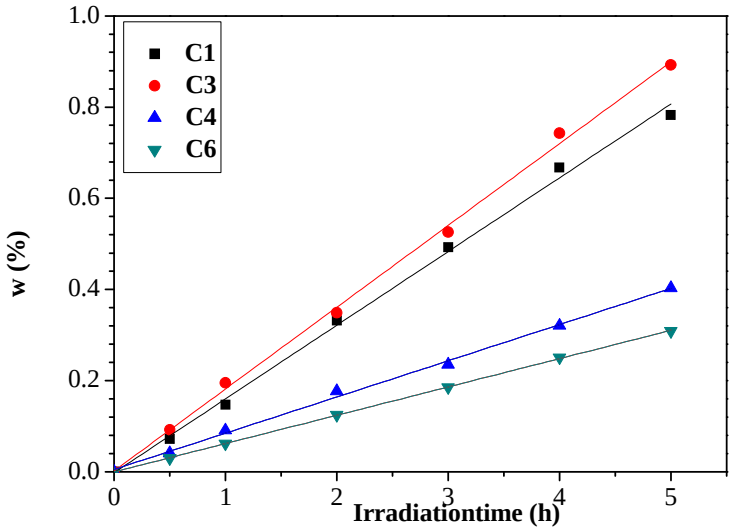

Figure 10

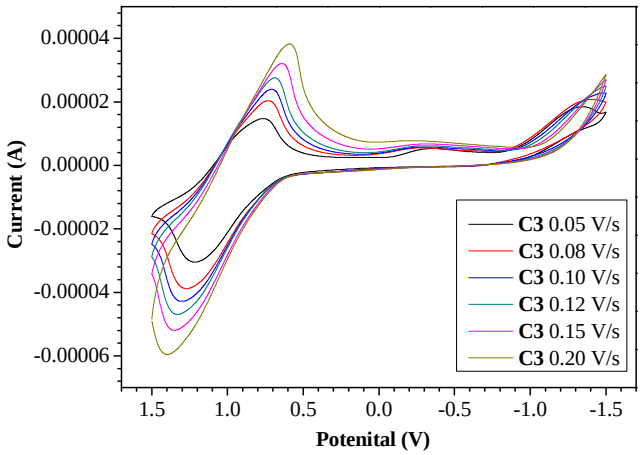

Figure 11

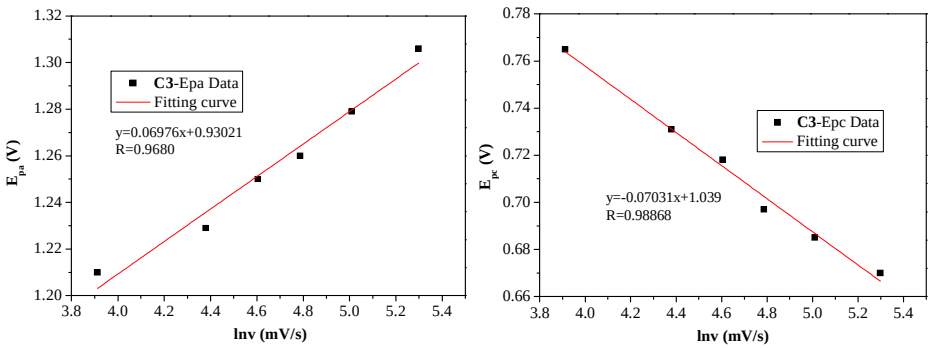

Highlights

- Synthesis of new conjugated dyes carrying dialkylamino and ketone groups through multi-step routes
- Visible light photoinitiating properties of these dyes using as one-component photoinitiators studied by photo-DSC
- Efficient visible light photoinitiating polymerization of methyl methacrylate by one-component photoinitiators
- Greater visible light photoinitiating efficiencies of one-component photoinitiators than two-component ones
- Triplet-triplet absorption of the new photoinitiators demonstrated by laser flash photolysis
- The production of free radicals trapped by ESR spectra